Acta Materialia 278 (2024) 120271

Contents lists available at ScienceDirect

Acta Materialia

journal homepage: www.elsevier.com/locate/actamat

Full length article

Experimental and computational assessment of the temperature dependency of the stacking fault energy in face-centered cubic high-entropy alloys

Konstantin V. Werner [a], Muhammad Naeem [b,c,*], Frank Niessen [a], Li Zhu [c], Matteo Villa [a], Xun-Li Wang [c,1], Marcel A.J. Somers [a,*]

[a] Department of Civil and Mechanical Engineering, Technical University of Denmark, Produktionstorvet, Building 425, Kongens Lyngby 2800, Denmark
[b] School of Metallurgy and Materials, University of Birmingham, Birmingham B15 2TT, United Kingdom
[c] Department of Physics and Center for Neutron Scattering, City University of Hong Kong, Kowloon, Hong Kong

ARTICLE INFO

Keywords:
Stacking fault energy
Twinning
Density functional theory
Deformation mode
High-entropy alloy

ABSTRACT

The activation of deformation mechanisms in face-centered cubic materials is considered closely related with the stacking fault energy. Experimentally determined stacking fault energy (SFE) values are exclusively positive. However, results obtained by first principle methods predict that the intrinsic SFE of metastable face-centered cubic metals and alloys is negative. It was previously shown that SFE values from the first principle methods and experiments can be reconciled by accounting for the resolved shear stress for Shockley partial dislocations. Determining this resolved shear stress for Shockley partial dislocations is experimentally challenging, making the reconciliation of experimental and first-principles SFE values a laborious exercise. In the present contribution, we demonstrate that the critical resolved shear stress for Shockley partial dislocations and SFE values can be determined from a single in-situ neutron diffraction experiment, thus enabling more confident and efficient reconciliation of experimental and theoretical SFE values.

1. Introduction

High- and medium-entropy alloys, HEAs and MEAs, respectively, have attracted considerable research interest due to their promising combination of ultimate tensile strength and ductility, even at cryogenic temperatures [1–5]. It is commonly claimed that HEAs and MEAs exhibit a higher intrinsic yield strength as compared to traditional structural materials, such as, e.g., austenitic (stainless) steels, due to an increase in average atomic misfit and associated type III lattice strains [6,7]. However, upon closer comparison of literature data this claim seems to be questionable as the difference in yield strength between HEAs and MEAs and austenitic (stainless) steel seems to be negligible [8–10]. In contrast, the high ductility of HEAs and MEAs is associated with twinning-induced plasticity (TWIP) and transformation induced plasticity (TRIP) effects [3,11,12], which provide more pronounced work hardening than dislocation slip and therefore delay the onset of necking. The reason for the increase in the work hardening rate associated with the TWIP and TRIP effect is considered to be the continuous refinement of the microstructure due to the formation of twin boundaries and martensite/austenite phase boundaries, which constitute obstacles for dislocation movement by the dynamic Hall-Petch effect [13,14].

Whether a material deforms by a combination of dislocation slip and TRIP/TWIP or by dislocation slip alone is thought to be governed by the stacking fault energy (SFE) [15,16]. The SFE is the energy associated with the presence of a stacking fault (SF) that forms in a face-centered cubic (*fcc*) matrix and is terminated by a pair of Shockley partial dislocations. Thermodynamically, the SFE can be modelled as a two-atomic layer thick ε–martensite embryo [17]. In the current paradigm, low experimental SFE values (<20 $mJ{\cdot}m^{-2}$) favor TRIP, while intermediate SFE values (20 – 40 $mJ{\cdot}m^{-2}$) lead to TWIP and materials with even higher SFE values (>40 $mJ{\cdot}m^{-2}$) deform exclusively by dislocation slip [15,18]. The SFE is commonly considered an intrinsic materials property, irrespective of whether it is experimental or thermodynamic, and depends on chemical composition, temperature and pressure [19–22].

* Corresponding authors.
E-mail addresses: m.naeem@bham.ac.uk (M. Naeem), majs@mek.dtu.dk (M.A.J. Somers).
[1] Xun-Li Wang was an Editor of the journal during the review period of the article. To avoid a conflict of interest, Xun-Li Wang was blinded to the record and another editor processed this manuscript.

https://doi.org/10.1016/j.actamat.2024.120271
Received 15 March 2024; Received in revised form 1 August 2024; Accepted 5 August 2024
Available online 6 August 2024

Following this paradigm, SFE can be used to tailor the combination of prevalent deformation mechanisms and hence the mechanical properties of an alloy.

Recent advances in first principle calculations challenge the assumption that plastic deformation of *fcc* metals and alloys is governed alone by their respective intrinsic SFE [23,24]. Instead, it appears that plastic deformation and the prevalence of certain deformation mechanisms is governed by the generalized stacking fault energy (GSFE) surface [23,24]. Theoretical (thermodynamic) SFE values from density functional theory (DFT) are systematically lower than SFE values determined by experiments and even become negative for metastable materials. This contradicts with the positive experimental SFE values [25–28]. Wei & Tasan [25] as well as Sun et al. [26] suggested that the experimental SFE determination neglects the resistance against the movement of Shockley partial dislocations, which effectively alters the force balance if taken into account. Molecular dynamics simulations by Shih et al. [29] confirmed that the solute drag experienced by Shockley partial dislocations has an effect on the stacking fault width and, therefore, on the experimentally determined SFE. Recently, it was demonstrated by Werner et al. [27,28] that the systematic gap between theoretical and experimental SFE values can be bridged by considering the resistance against the movement of Shockley partials (τ_P) in the force balance over a stacking fault. Pragmatically, this resistance was postulated to be proportional to the critical resolved shear stress (CRSS) for twinning (τ_{Twin}), since τ_P cannot be easily assessed. This approach yielded unprecedented quantitative agreement between theoretical and experimental SFE values for both stable and metastable *fcc* materials (including HEAs and MEAs). Thus, a method for the simultaneous determination of τ_P (or τ_{Twin}) and SFE is sought for.

Transmission electron microscopy (TEM) is commonly used to determine τ_{Twin} by observing the onset of deformation twinning ex-situ or in-situ [4,11]. However, the experimental work associated with determining τ_{Twin} after ex-situ loading is laborious and the accuracy of the determined values for τ_{Twin} is directly related to the chosen stress/-strain intervals. On the other hand, in-situ TEM provides the opportunity to observe the motion of isolated Shockley partial dislocations and therefore the determination of τ_{Twin}/τ_P. However, investigating a vast compositional space with in-situ TEM is certainly not possible and findings indicate that the mechanical behavior of a thin foil cannot be translated easily to that of a bulk material [30]. Wang et al. [31] pointed out an alternative to determine τ_P, by probing the stacking fault probability (SFP) in-situ with X-ray or neutron diffraction during plastic deformation and infer τ_P from the relation between SFP and true stress.

This work aims to validate a previously proposed hypothesis, which demonstrates that the discrepancy between experimental and theoretical SFE values is due to the resistance to the motion of Shockley partial dislocations. Although the hypothesis showed unprecedented agreement between experimental and theoretical SFE values, it relies on experimental data, which is usually obtained from separate experiments. This does not only require a significant experimental workload, but also increases the uncertainty of the hypothesis results. In an attempt to reduce the experimental effort needed and increase the reliability of the hypothesis, it is shown for the example of FeCoCrNi, deformed in tension at different temperatures, that all necessary experimental data can be derived from a single in-situ neutron diffraction experiment. The correlation of experimental data and results obtained from DFT, demonstrates that the suggested approach enables for sub-zero temperatures a reconciliation of experimental and theoretical SFE values with a considerably reduced workload.

2. Experimental methods

2.1. Material

The FeCoCrNi samples were prepared from pure metals by arc-melting. To ensure chemical homogeneity, the materials were re-melted several times and subsequently cast into Cu-molds. Homogenization was performed in an argon atmosphere for 24 h at 1200 °C with subsequent quenching into water. The samples were cold-rolled to a thickness reduction of ~80% and afterwards annealed at 800 °C for 1 h to achieve full recrystallization, which resulted in an average grain size of approximately 5 μm. Tensile specimens with gauge dimensions of 25 mm × 4 mm × 3 mm were machined by wire electrical discharge machining from the as-recrystallized material.

2.2. Neutron diffraction and analysis of diffraction data

The in-situ neutron diffraction (ND) experiments were performed at the TAKUMI Engineering Materials Diffractometer, beamline-19 of the Materials and Life Science Experimental Facility at the Japan Proton Accelerator Research Complex. Low-temperature experiments were carried out with the cryogenic loading machine [32]. The tensile direction was inclined 45 ° relative to the incident neutron beam. Diffractograms were thus acquired with scattering vectors parallel to and normal to the tensile direction on the two detector banks, which are installed at –90 ° and +90 ° with respect to the incident neutron beam. Thus, during the in-situ tensile tests, the data was acquired along both loading and transverse directions. Temperatures were monitored with a Chromel/AuFe0.07% thermocouple that was fixed to the gauge part of samples. Prior to loading, the samples were cooled and held for ~1 h at low temperatures (25 K, 40 K and 140 K). Tensile loading was applied at a strain rate of 2.67×10^{-5} s^{-1}.

Rietveld refinement of the diffractograms was performed with the Z-Rietveld software [33]. The lattice strain for individual lattice planes ε_{hkl} was obtained from:

$$\varepsilon_{hkl} = \frac{(d_{hkl} - d^0_{hkl})}{d^0_{hkl}} \tag{1}$$

where d_{hkl} is the lattice spacing of the *{hkl}* family of lattice planes upon loading and d^0_{hkl} is the strain-free lattice spacing. The SFP was determined using first and second order *{hhh}* reflections applying Warren's method [34]:

$$SFP = \frac{32\pi}{3\sqrt{3}}(\varepsilon_{222} - \varepsilon_{111}) \tag{2}$$

with ε_{111} and ε_{222} the lattice strains for {111} and {222} parallel to the loading direction, respectively.

Experimental stacking fault energies (γ^{Exp}_{isf}) were calculated with the equation proposed by Reed and Schramm [35]:

$$\gamma^{Exp}_{isf} = \frac{6.6 a_0 G_{111}}{\pi\sqrt{3}} \frac{\langle \varepsilon^2_{111} \rangle}{SFP} A^{-0.37} \tag{3}$$

where G_{111} is the shear modulus in the {111} plane, a_0 is the lattice parameter, A is the Zener anisotropy, and $\langle \varepsilon^2 \rangle_{111}$ is the mean-square strain in the [111] direction.

2.3. Materials characterization

The microstructure was investigated on the tested (until fracture) specimens on a JEOL JEM-2100F transmission electron microscope (TEM). Samples were prepared by focused ion beam (FIB) milling, using an FEI Scios DualBeam SEM/FIB system. To prevent beam damage the FIB lamellae were capped with a protective platinum (Pt) deposit. Gallium (Ga^+) ion beams of 5 nA at 30 kV and 0.1 nA at 30 kV were used for sample-cutting and early-stage milling, respectively. Finally, Ga^+-ion beams of 23 pA at 16 kV and 4.3 pA at 2 kV were used as to minimize the introduction of artefacts in the final preparation step.

3. Computational methods

The SFE values for the FeCoCrNi alloy at the four test temperatures were calculated using Density Functional Theory (DFT) modeling and the Coherent Potential Approximation (CPA) [36,37] as implemented in the exact muffin-tin orbitals (EMTO) package [37,38]. The paramagnetic state of the alloys was accounted for using the disordered local magnetic moment (DLM) method [39]. The *fcc* lattice was modelled using nine *(111)* planes consisting of one atom each and stacked in the standard sequence *ABCABCABC*. The lattice vectors of the *fcc* cell were $a_1 = a_0\langle 101\rangle/2$, $a_2 = a_0\langle 011\rangle/2$ and $a_3 = a_0\ \sqrt{3}\langle 111\rangle/3$, where a_0 is the *fcc* lattice parameter. Shifting a_3 by $a_0\ \langle 11\bar{2}\rangle/6$ introduces an intrinsic stacking fault via the periodic boundary condition to produce the new stacking sequence *ABCABCABC* | *BCABC* …. The stacking fault energy was then obtained from:

$$\gamma_{isf}^{DFT} = \left(F_{SF} - F_{fcc}\right)\Big/A \tag{4}$$

with F_{fcc} and F_{SF} the Helmholtz energies of the supercells, respectively before and after introducing a stacking fault of area A. The Helmholtz energies consisted of the DFT total energy and the magnetic entropy contribution as applied in Ref. [40]. First-principles calculations were conducted at the atomic volumes derived from the experimental lattice parameters at the test temperatures to partially account for the effect of a finite temperature. The exchange-correlation functional was approximated using the Perdew, Burke, and Ernzerhof (PBE) generalized gradient approximation [41]. The resolution of the k-point mesh was tested for energy convergence and consisted of 10,556 uniformly distributed points with an error of < 0.1 mJ·m^{-2} in SFE.

4. Results

4.1. Mechanical properties

The mechanical properties of the FeCoCrNi HEA tested at four different temperatures were reported and evaluated in detail elsewhere [42]. Key mechanical parameters as well as the lattice parameter of the undeformed HEA are given in Table 1.

It is apparent that lowering the deformation temperature enhances the mechanical properties of the FeCoCrNi HEA significantly; yield strength (σ_y) and ultimate tensile strength (σ_{UTS}) increase by a factor of 2 and 2.4, respectively, on reducing the deformation temperature from 295 K to 25 K. In addition, the strain at failure (ε_f) increases from 45.0% at 295 K to 58.7% at 140 K and appears to remain unchanged for deformation temperatures below 140 K. The observed improvement in mechanical properties of the FeCoCrNi HEA at cryogenic temperatures agrees with the correlation of deformation temperature and mechanical properties of HEAs reported in the literature [3,4]. Lowering the deformation temperature is considered to result in a drastically higher thermal contribution to the Peierls stress, hence rendering solid solution strengthening more potent at low temperatures [42]. Below room temperature, the Hall-Petch coefficient depends only weakly on temperature, such that its contribution is negligible as compared to the Peierls stress contribution [43]. The improved ductility of HEAs and MEAs at low temperatures is attributed to a larger contribution of the TWIP effect [8], which increases the work hardening rate as a result of the dynamic Hall-Petch effect [11,44].

Table 1
Mechanical properties of the FeCoCrNi alloy for the four test temperatures 25 K, 40 K, 140 K, and 295 K. Yield strength (σ_y), ultimate tensile strength (σ_{UTS}), strain at failure (ε_f), contribution of work hardening (θ), and the strain-free lattice parameter (a_0) [42].

Temperature [K]	σ_y [MPa]	σ_{UTS} [MPA]	ε_f [%]	θ [MPa]	a_0 [Å]
295	331	1009	45.0	678	3.5723
140	502	1886	58.7	1384	3.5644
40	637	2377	58.9	1740	3.5637
25	676	2396	58.4	1720	3.5636

4.2. Microstructural evolution upon plastic deformation

Diffractograms of the HEA in undeformed condition and at σ_{UTS} for the four investigated temperatures are given in Fig. 1a–d. In undeformed condition the HEA diffractograms only reveal an *fcc* structure with sharp peaks, irrespective of temperature.

The diffractograms of the HEA specimens at σ_{UTS} do not reveal additional peaks, indicating that the FeCoCrNi HEA is thermodynamically stable under deformation and does not form martensite. This is in line with previous investigations that confirm the absence of deformation-induced martensite in FeCoCrNi deformed at cryogenic temperatures [31,42]. The bright-field TEM images in Fig. 2 confirm that FeCoCrNi remains *fcc* at cryogenic temperature and that deformation twins develop. In contrast to the findings by Wang et al. [31], the sample deformed at 295 K did not show indications of deformation twinning. Absence of twinning at 295 K is attributed to the relatively small grain size of the FeCoCrNi HEA in this work as compared to the FeCoCrNi samples investigated by Wang et al. [31]. A small grain size has been demonstrated to reduce the propensity for, and eventually fully suppresses, twinning [45–49], because the CRSS for twinning is inversely proportional to grain size [45,50].

4.3. Evolution of the stacking fault probability with true stress

The evolution of the stacking fault probability for the four test temperatures, determined according to Eqs. (1),(2) is given in Fig. 3a – d as a function of the true stress. Comparing the SFP vs. true stress curves, reveals three distinctive aspects: i) the achievable magnitude of the SFP is temperature dependent, such that a lower deformation temperature results in a higher SFP, ii) initially the SFP remains approximately zero, but starts to increase beyond a threshold stress, iii) the rate at which SFP increases with true stress depends on temperature.

In line with the trends reported in the literature [31,51,52], the SFP attained at fracture decreases with increasing temperature from approx. $45{\cdot}10^{-3}$ at 25 K and 40 K to $5{\cdot}10^{-3}$ at 295 K. Evidently, lowering the deformation temperature eases stacking fault and twin formation, as corroborated by TEM (cf. Fig. 2) and thus augments their contributions to strain hardening [42,51]. Intriguingly, in the temperature range 25 K to 140 K the SFP increases at 0.028 MPa^{-1} with true stress at virtually the same rate, while at 295 K it is only one third of this rate: 0.009 MPa^{-1}. Certainly, this indicates that SF formation is promoted by a lower deformation temperature.

The threshold stress beyond which SFP increases was determined from Fig. 3 by fitting the data points with a piecewise linear function and is taken as the critical stress for widening of the SFs (σ_P). The determined values for σ_P are compared with the yield stress σ_y in Fig. 4. Clearly, the difference between σ_y and σ_P becomes smaller with decreasing temperature, in agreement with findings by Kireeva et al. [53–56] and Abuzaid & Sehitoglu [57], who stated that lowering the deformation temperature shifts the onset of twinning to lower plastic strains and higher stresses.

4.4. Stacking fault energy as a function of temperature

For increasing true stress, the determined SFE value asymptotically approaches a certain value (Fig. 5a–d). A similar dependence of γ_{isf}^{Exp} on the true stress has been reported previously for HEAs/MEAs and for stainless steels [31,51,52]. In line with literature, the average values for these steady state regimes are taken as the experimental SFE values (see the horizontal dashed lines in Fig. 5 [31,51,52]). Evidently, at 295 K the steady state regime is not yet reached (Fig. 5d). Therefore, pragmatically

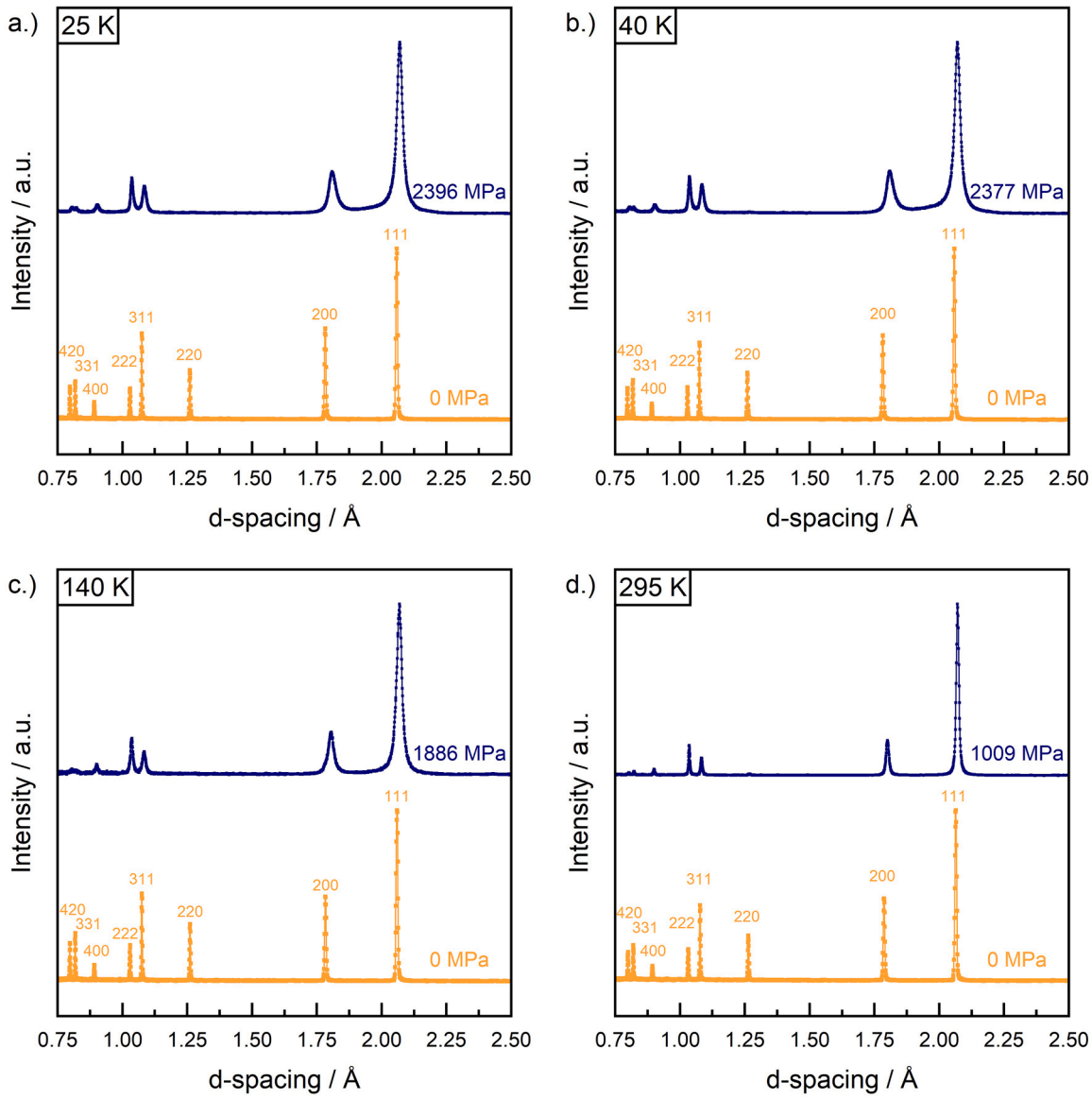

Fig. 1. Normalized diffractograms of the FeCoCrNi HEA in the undeformed state, and upon reaching the ultimate tensile strength – a. 25 K, b. 40 K, c. 140 K and d. 295 K.

the lowest SFE value is taken as the experimental SFE. It is reasoned that the absence of a plateau for 295 K is consistent with the limited strain hardening at this temperature, which prevents wide stacking faults from forming.

The experimental SFE values in Fig. 6 show a non-linear dependence on temperature and approach a constant value, for temperatures up to (at least) 140 K. This behavior resembles the experimental SFE values of Cu-Al alloys that exhibit an asymptotic trend towards a constant, positive value for increasing Al-content. This asymptotic behavior was demonstrated to be a consequence of the aforementioned, incomplete force balance over a stacking fault that biases positive experimental SFE values [26,28]. SFE values for the FeCoCrNi have not been reported before for temperatures as low as 25 K and 40 K. The SFE value of 36 $mJ{\cdot}m^{-2}$ at 295 K (c.f. Table 2) is slightly higher than the values reported earlier in the literature, which are in the range 27 – 32.5 $mJ{\cdot}m^{-2}$ [31,58,59]. A slightly higher SFE value may originate from the small grain size in the investigated samples. Experimentally determined (apparent) SFE values depend on the grain size by a Hall-Petch type dependence, so smaller grains have a higher experimental SFE value [27,49,60]. The error bar for the 295 K specimen in Fig. 6 reflects the estimated error as a consequence of the procedure to determine γ_{isf}^{Exp} in Fig. 5d.

In contrast to the positive experimental values, the theoretical DFT values are negative and increase linearly with temperature at 0.025 $mJ{\cdot}m^{-2}{\cdot}K^{-1}$. This value is commensurate with the temperature dependence of SFE reported for stainless steels and HEAs [61,62]. The negative SFE values obtained from DFT illustrate that experimental validation of DFT simulations is not straightforward. It is noted that DFT values calculated for the SFE at 25 K and 40 K are higher than the typical values reported in the literature for 0 K [26]. Generally, DFT SFE values at 0 K are derived from the DFT ground-state volume, which yields an underestimate of the actual lattice parameter [26,63]. By means of example, for the room temperature sample investigated here, taking the lattice parameter as 3.577 Å (experimental value used in Ref. [26]) instead of 3.5723 Å (experimental value in the current work), changes γ_{isf}^{DFT} from −7.5 $mJ{\cdot}m^{-2}$ to −1 $mJ{\cdot}m^{-2}$, corresponding to the SFE value for FeCoCrNi reported by Xun et al. [26]. Analogously, results by Niessen et al. [64] demonstrated that the lattice parameter has a significant influence on the SFE values calculated with DFT. On comparing experimental and theoretical SFE values, it is essential that the experimental lattice parameter is used for both values.

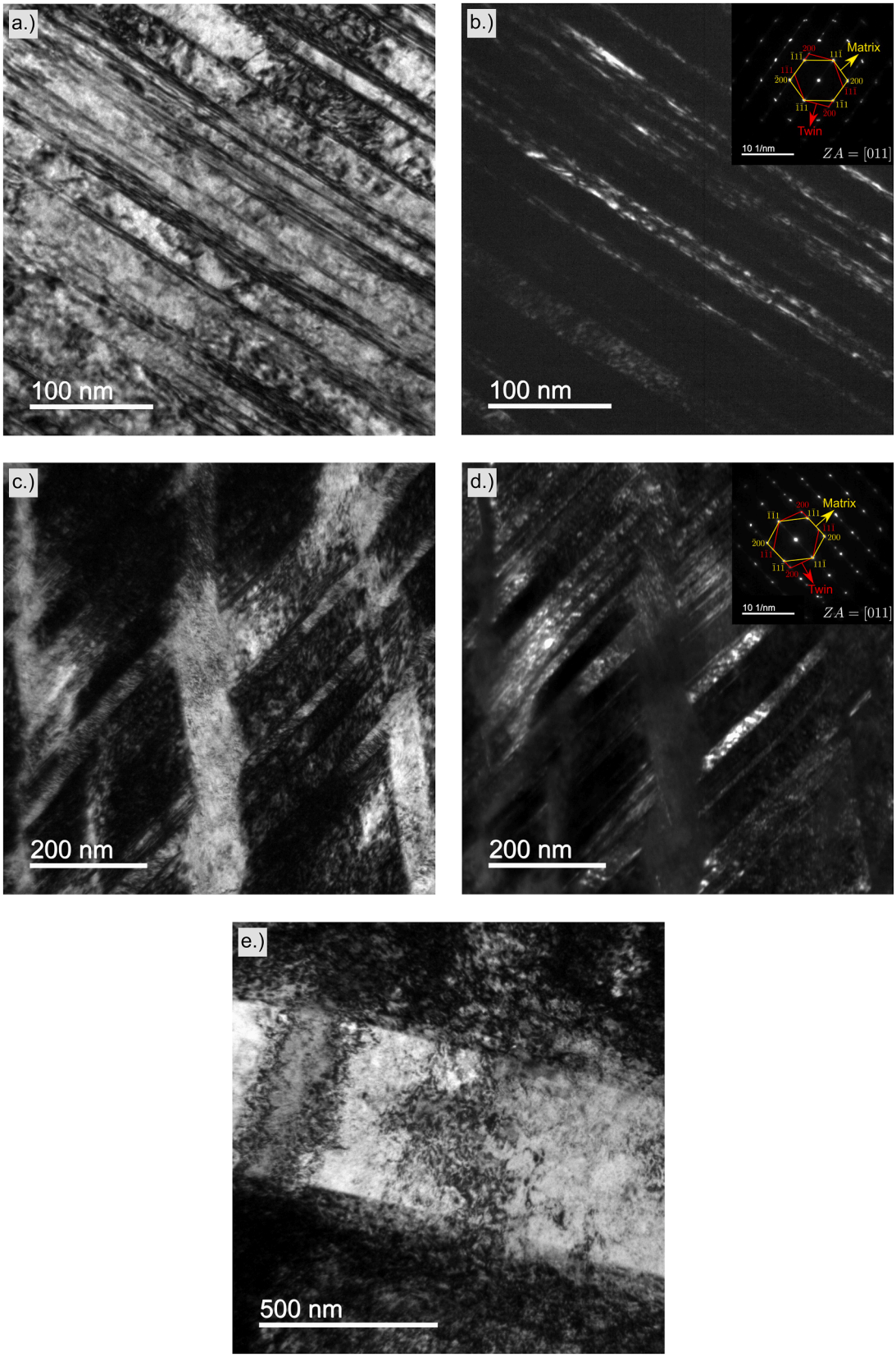

Fig. 2. Bright field images obtained by transmission electron microscopy of the as-fractured FeCoCrNi HEA samples tested at – a. 25 K, c. 140 K and e. 295 K. Dark field images and the corresponding selected area diffraction patterns are given in – b. 25 K and d. 140 K. Images were taken very close to the fracture.

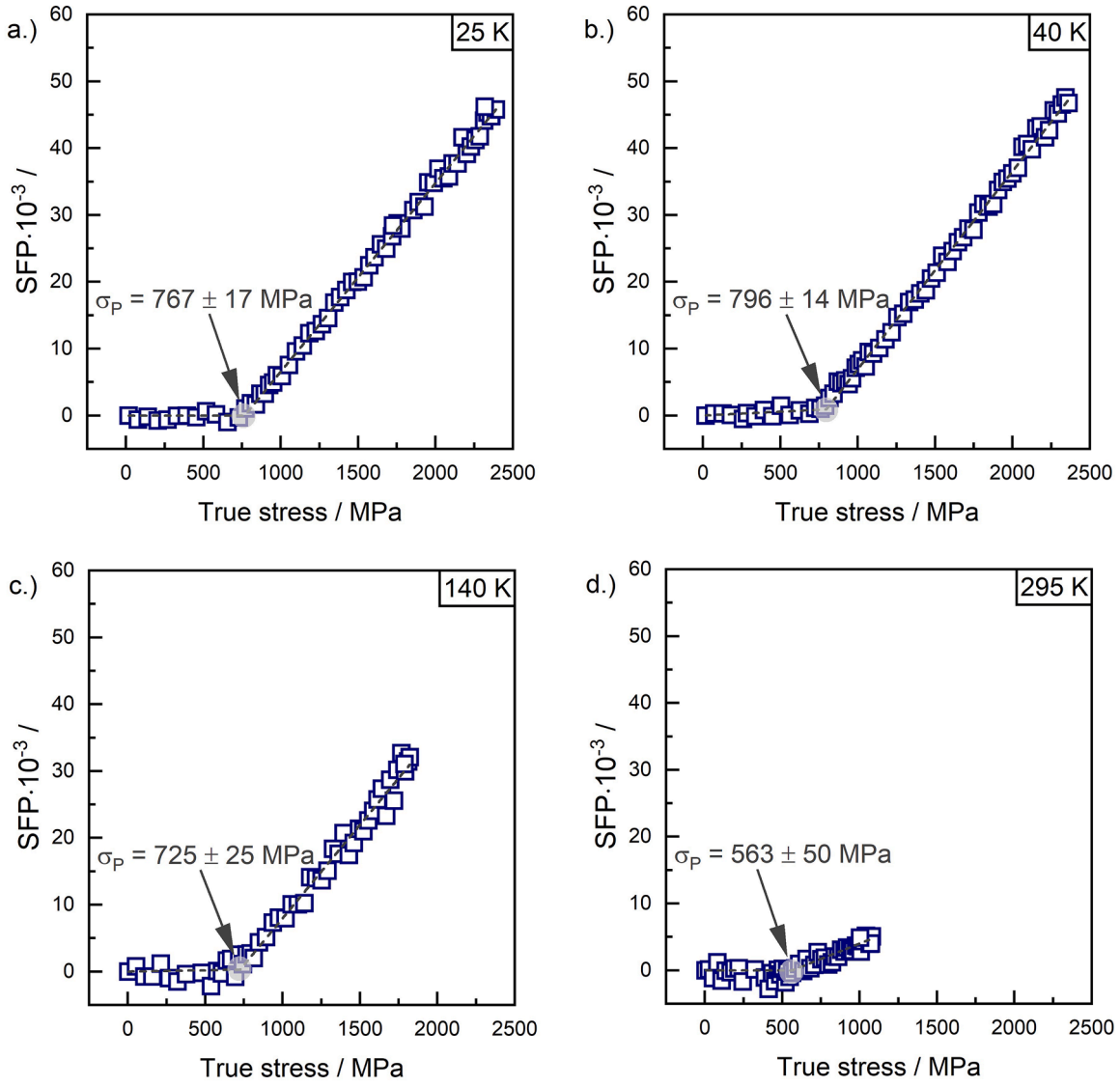

Fig. 3. Stacking fault probability (SFP) determined according to Eq. (2) as a function of the true stress for the four different deformation temperatures – a. 25 K, b. 40 K, c. 140 K and d. 295 K.

5. Discussion

5.1. Critical resolved shear stress for twinning as a function of temperature

In their review on the mechanical properties of HEAs and MEAs, George et al. [65] thoroughly addressed the effect of temperature on the twinning stress. The literature on this topic reports two irreconcilable observations. Certain investigations claim an increase in twinning stress with decreasing deformation temperature [53–57], while others report that the twinning stress is insensitive to temperature, or even decreases with decreasing deformation temperature [4,11,31,44,52].

The observations of insensitivity or decreasing twinning stress upon lowering the deformation temperature in HEAs and MEAs commonly rely on ex-situ TEM investigations of polycrystalline materials [4,11,44]. This approach has two sources of uncertainty. Firstly, the accuracy with which the onset of twinning can be detected with this method depends on the stress/strain intervals at which the ex-situ TEM characterization is performed. This becomes especially critical when the work hardening rate increases at a lower deformation temperature. Consequently, the stress/strain intervals should be selected along with the deformation temperature, meaning that for a lower temperature the interval between successive measurements should be reduced to guarantee an accurate critical twinning stress. Secondly, since deformation twinning is orientation dependent, the Schmid factor of the active/observed twin system is required to determine the twinning stress unambiguously. In ex-situ TEM, relating the crystal orientation under investigation to the loading direction is challenging. Therefore, the CRSS is often obtained from dividing the applied stress by the Taylor factor [4,11,44]. This may contribute to uncertainty in the determined twinning stress, despite preparation of TEM foils with a surface normal inclined 45 ° relative to the loading direction as by Laplanche et al. [4].

Claims of an increasing twinning stress upon lowering the deformation temperature are often derived from ex-situ TEM observations of twinning in single crystals [53–57]. For single crystals the orientation dependence of twinning can be properly accounted for, but the selected stress/strain intervals in relation to temperature are still a source of uncertainty.

As noted by George et al. [65], in addition to the conflicting groups of experimental results, none of the models presented to date correctly describes the twinning stress for a wide range of different *fcc* materials. The only hypothesis that seems to yield reliable predictions for the twinning across a wide range of different alloys, [27,28], assumes that the twinning stress multiplied by the Burgers vector of Shockley partial

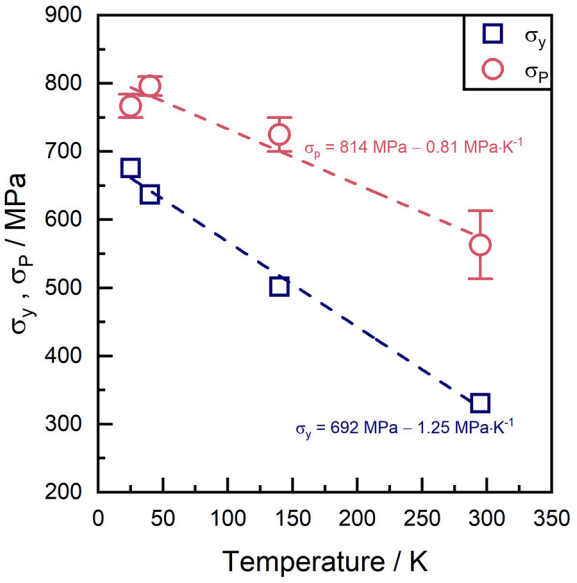

Fig. 4. Yield strength (σ_y) and critical stress for widening of stacking faults (σ_P) as a function of the deformation temperature. The dashed lines are given to guide the eye.

dislocations reconciles experimental and theoretical SFE values:

$$\gamma_{isf}^{Exp} = \gamma_{isf}^{DFT} + b_p \tau_{Twin} \tag{5}$$

Eq. (5) can then be rearranged to:

$$\tau_{Twin} = \frac{\gamma_{isf}^{Exp} - \gamma_{isf}^{DFT}}{b_p} \tag{6}$$

The hypothesis presumes pragmatically that the twinning stress equals the stress required to separate two Shockley partial dislocations. According to Eq. (6), τ_{Twin} can be calculated from γ_{isf}^{Exp} and γ_{isf}^{DFT}. Using the values in Table 2, τ_{Twin} decreases with decreasing temperature, as shown in Fig. 7a. This would be in disagreement with an increase of σ_P for decreasing temperature, cf. Fig. 4. However, as discussed by Kubilay & Curtin [66] τ_P, and hence also σ_P, comprise terms related to both the propagation of SFs and their nucleation. Hence, the apparent contradiction between the temperature-trends of σ_P (Fig. 4) obtained from experiments and τ_{Twin} (Fig. 7a) derived from Eq. (6), may result from the fact that experimental values for σ_P comprise both nucleation and propagation barriers.

Steinmetz et al. [67] presented a model for the critical resolved shear stress for deformation twinning that assumes propagation control:

$$\tau_{Twin} = \frac{\gamma_{isf}^{Exp}}{3b_p} + \frac{3Gb_p}{L} \tag{7}$$

where L is the twin embryo length. Assuming a value of $L = 260\ nm$, the values determined for τ_{Twin} (orange circles in Fig. 7a) agree excellently with the values determined according to Eq. (6) in the temperature range up to (at least) 140 K. This agreement strongly supports the suggestion that the difference between γ_{isf}^{DFT} and γ_{isf}^{Exp} arises from the propagation barrier for wide stacking fault / twin formation [27,28]. Furthermore, the results suggest that twinning in the FeCoCrNi MEA is propagation controlled at sub-zero temperatures where γ_{isf}^{DFT} becomes more negative. This suggestion concurs with observations in Cu-Al alloys reported by Tranchant et al. [68], where the rate controlling step for twinning changes from nucleation to propagation for an Al-content of approximately 8 – 10 at.%. Notably, in this composition interval γ_{isf}^{DFT} changes from a positive (for lower Al contents) to a negative value [28].

The question remains, whether the experimentally determined values for σ_P, and therefore τ_P, can be reconciled with the values for τ_{Twin} by distinguishing between the propagation and nucleation barriers. According to Kubilay & Curtin [66] as well as Kireeva et al. [55], τ_P is given by:

$$\tau_P = \tau_{Nuc} + \tau_P^{SS}(T, \dot{\varepsilon}) \tag{8}$$

with $\tau_{Nuc} = \frac{\gamma_{isf}^{Exp}}{b_p}$ [66]:

$$\tau_P = \frac{\gamma_{isf}^{Exp}}{b_p} + \tau_P^{SS}(T, \dot{\varepsilon}) \tag{9}$$

where $\tau_P^{SS}(T, \dot{\varepsilon})$ is the propagation barrier of Shockley partial dislocations arising from solid solution strengthening and thus depends on deformation temperature (T) and strain rate ($\dot{\varepsilon}$). Hence, the propagation barrier of Shockley partials can, according to Eq. (8), be obtained by multiplying the values of σ_P with the respective Schmid factor for the leading Shockley partial (m_L) and subsequent subtraction of the nucleation term:

$$\tau_P^{SS}(T, \dot{\varepsilon}) = m_L \sigma_P - \frac{\gamma_{isf}^{Exp}}{b_p} \tag{10}$$

The Schmid factor values for leading and trailing (m_T) Shockley partial dislocations as well as dislocation glide (m) are given in Table 3 as a function of the crystal orientation parallel to the loading direction.

The values for τ_P^{SS} obtained from Eq. (10) are given in Fig. 7b together with the critical resolved shear stress of the Shockley partials (τ_P) and τ_{Twin} obtained from Eq. (6). For the deformation temperatures 25 K, 40 K, and 140 K, the values for τ_P^{SS} are in good agreement with the predicted values from Eq. (6). This indicates that for materials that form wide SFs and/or deformation twins during deformation, in-situ ND or XRD experiments can yield reliable values for the SFE as well as the critical resolved shear stress for SF-formation. For the 295 K specimen, τ_P =175 ± 15 MPa, which is not only significantly lower than the value for τ_{Twin} obtained from Eq. (6), but also lower than experimentally determined room-temperature values for τ_{Twin} for HEAs and MEAs with similar SFE and grain size. Concerning the latter, Wagner & Laplanche [69] determined $\tau_{Twin} = 260 \pm 18$ MPa for the classical Cantor alloy with a grain size of 6 μm. This value corresponds well to the value obtained from Eq. (6): $\tau_{Twin} = 295 \pm 42$ MPa. Given the significant difference between the experimental values for τ_P and the results from Eq. (6), it appears plausible that, at least for the 295 K specimen, the apparent threshold stress in Fig. 1 does not correspond to the formation of wide SFs. This is further corroborated by the significantly lower slope of the SFP vs. true stress curve and absence of deformation twins (Fig. 2e).

Based on the experimental data it is not possible to unambiguously assess a clear relation between stacking fault energy and the twinning propensity/stress. This is mostly related to the 295 K value for σ_P, which is 563 ± 50 MPa. Based on the sub-zero temperature values for σ_P, one might conclude that the twinning stress is athermal. On the other hand, taking the 295 K value into account, the data points towards thermally activated stacking fault formation, at least partially, and hence thermally activated twinning. These observations related to temperature dependence of the twinning stress can be discussed speculatively, as follows.

Assuming that the critical stress for twinning can be described by Eq. (8), it comprises a component related to the nucleation barrier of a stacking fault and the propagation barrier term. The propagation barrier expresses how difficult it is for the Shockley partial dislocations to move. The nucleation term expresses how easy it is to form a stacking fault, which is thought to be dominated by the thermodynamics of the system. This means that the more metastable an *fcc* material is, the higher is its driving force for stacking fault formation, while the propagation term stands for the kinetics of stacking fault formation. At lower

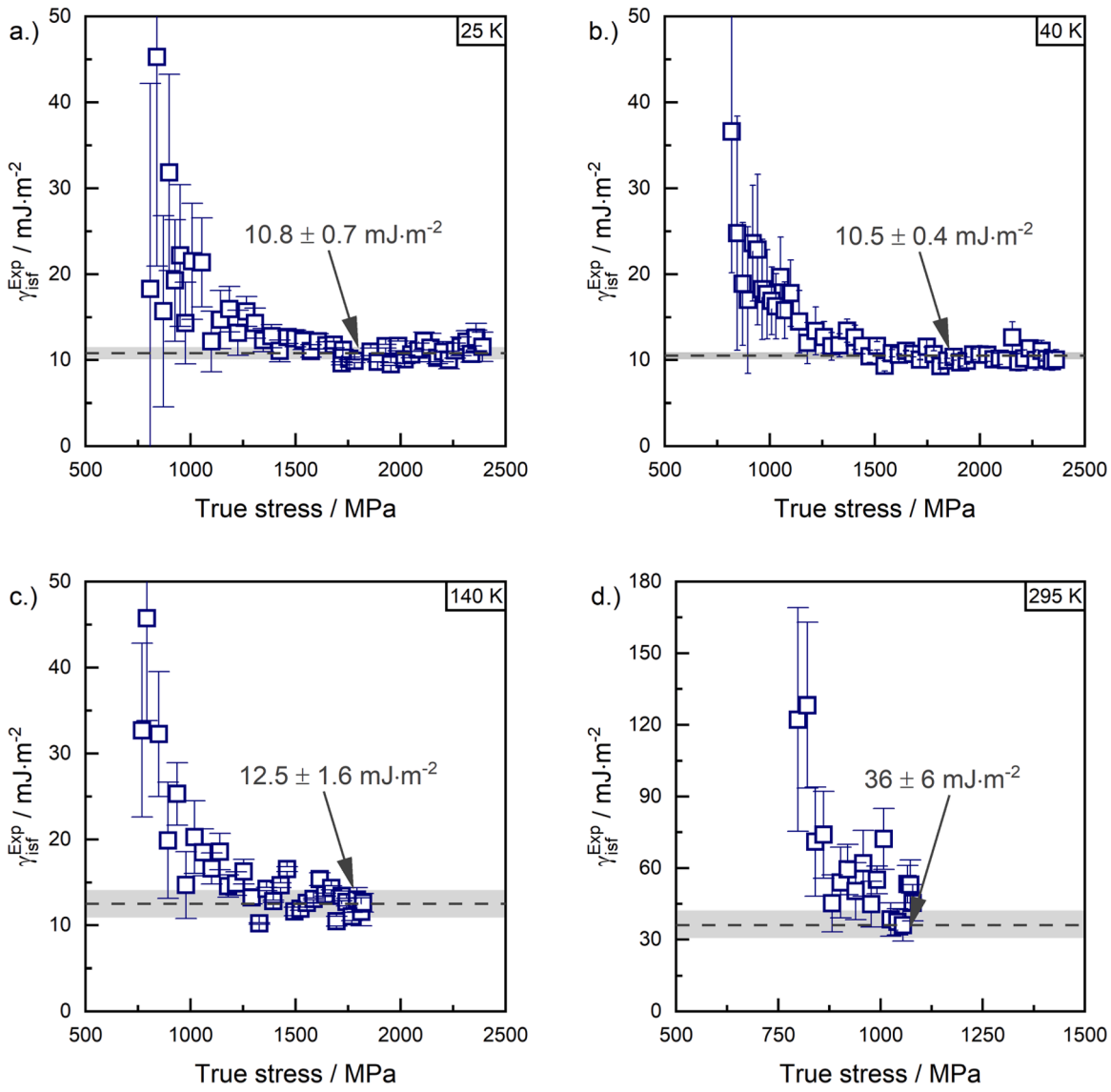

Fig. 5. Stacking fault energy (γ_{isf}^{Exp}) determined according to Eq. (3) as a function of the true stress for the four different deformation temperatures – a. 25 K, b. 40 K, c. 140 K and d. 295 K.

temperatures, the driving force for stacking fault formation in metastable systems should increase because the difference in Gibbs energy between *fcc* austenite and *hcp* $\varepsilon-$ martensite increases. This would imply a proportional relationship between twinning stress and SFE. However, the resistance against the movement of the Shockley partial dislocations should, as it does for perfect dislocations, increase with decreasing temperature, which in turn would hint towards an increase in twinning stress at lower temperatures. As mentioned, the critical twinning stress comprises both nucleation and propagation terms. Hence, it can be speculated that pseudo-athermal behavior is observed if the temperature dependent contributions to nucleation and propagation terms cancel each other. The available data cannot prove this hypothesis. Nevertheless, conceiving deformation twinning and formation of deformation-induced martensite in terms of temperature dependent contributions of the thermodynamics and the kinetics of stacking fault formation, may contribute to improved understanding of these mechanisms and may pave the road towards designing materials with competitive combinations of strength and ductility.

Further explanations for the lack of agreement between the three independent methods for the room temperature specimen (cf. Fig. 7b) are the following. Firstly, the γ_{isf}^{Exp} versus true stress curve displayed in Fig. 6d did not yet reach a plateau value, so the actual value for γ_{isf}^{Exp} might be lower than the estimated 36 mJ·m^{-2}. By means of example, using Eq. (6) a discrepancy of 6 mJ·m^{-2} in γ_{isf}^{Exp} corresponds to a variation of 42 MPa in τ_{Twin}. Secondly, the uncertainty of σ_P, as established from the piecewise linear fit, is greater for the 295 K specimen than for the specimens tested at cryogenic temperatures (cf. Fig. 4). Thirdly, the DFT calculations are expected to have a higher level of uncertainty for elevated temperatures than for temperatures close to 0 K.

5.2. Assessment of SFE by in-situ diffraction techniques

In-situ ND and/or XRD experiments represent a robust methodology for investigating the deformation mechanisms in metallic materials, facilitating the determination of the SFE utilizing the Reed & Schramm method [35]. Nevertheless, it is imperative to exercise caution interpreting the findings, as exemplified by the outcomes of this investigation.

Firstly, the specimen deformed at 295 K does not (yet) reach a plateau in the SFE versus true stress relationship, while specimens tested at sub-zero Celsius temperatures did reach a steady-state at a true stress

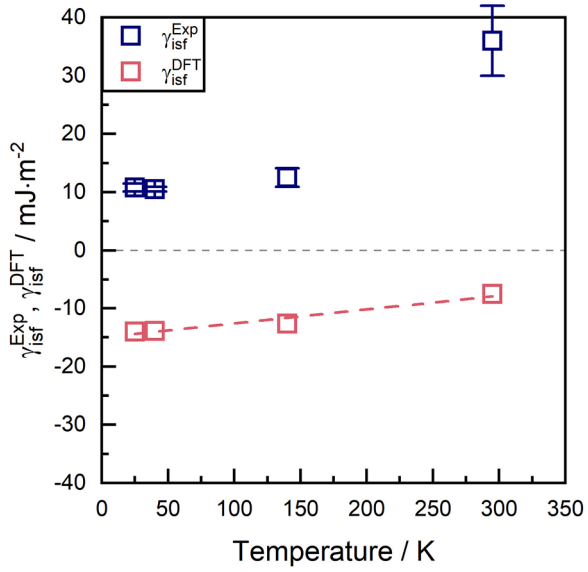

Fig. 6. Experimental (γ_{isf}^{Exp}) and theoretical stacking fault energy (γ_{isf}^{DFT}) of the FeCoCrNi samples as a function of temperature.

Table 2
Stacking fault energy values of the FeCoCrNi specimens determined by DFT (γ_{isf}^{DFT}) and neutron diffraction (γ_{isf}^{Exp}).

	Temperature [K]			
	295	140	40	25
γ_{isf}^{DFT} [mJ·m^{-2}]	−7.5	−12.6	−13.9	−14
γ_{isf}^{Exp} [mJ·m^{-2}]	36	12.5	10.5	10.8

roughly twice that of σ_P (cf. Figs. 3 and 5). This observation underscores the necessity for sufficient strain hardening to enable the development of wide stacking faults within the probed crystallites. This precondition is aligned with Warren's theory [34] that forms the basis of the Reed & Schramm method in Eq. (3) [35]. Not meeting this criterion can result in experimental SFE values obtained via ND and/or XRD that deviate from those acquired by TEM analysis.

Furthermore, the determination of stacking fault probabilities relies on analyzing the peak shifts associated with specific crystallographic planes, such as {111} and {222} (see Eq. (2)), or {111} and {200} planes [70], respectively. However, the selection of these crystallographic planes is of paramount importance.

In the case of {111} and {222} planes, the Schmid factors for the Shockley partial dislocations are identical, both for leading and the trailing partials. Thus, the alignment of the probed planes relative to the tensile axis implies an expansion of stacking faults. Conversely, on investigating {111} and {200} planes, cf. Table 3, the dynamics is different. Stacking faults in crystallites oriented along ⟨200⟩ parallel to the tensile axis undergo contraction under applied stress. Consequently, the stacking fault probabilities in crystallites oriented along ⟨111⟩ and ⟨200⟩ will diverge. This phenomenon is inconsistent with Warren's method, which assumes uniform fault densities across all crystallites [34,71]. Given these considerations, it is advisable to consider how the selection of crystallographic planes impacts experimental stacking fault energy values.

5.3. Correlation between stacking fault energy and prevailing deformation mechanism(s)

According to the DFT calculations, *fcc* FeCoCrNi is metastable ($\gamma_{isf}^{DFT} < 0$) for all investigated deformation temperatures and should thus, according to Olson & Cohen [17], have a driving force to form martensite on deformation. However, the diffractograms in Fig. 1 show that the specimens retain their *fcc* lattice during deformation, irrespective of the deformation temperature. The absence of a strain-induced martensitic transformation was earlier observed in other metastable HEAs and MEAs, such as CoCrFeMnNi [5] and

Table 3
Schmid factor values for leading (m_L) and trailing (m_T) Shockley partial dislocations as well as dislocation glide (m) depending on the crystallographic orientation of the tensile axis.

Crystal orientation	Schmid factor		
	m	m_L	m_T
<111>	0.27	0.31	0.16
<110>	0.41	0.47	0.23
<100>	0.41	0.24	0.47

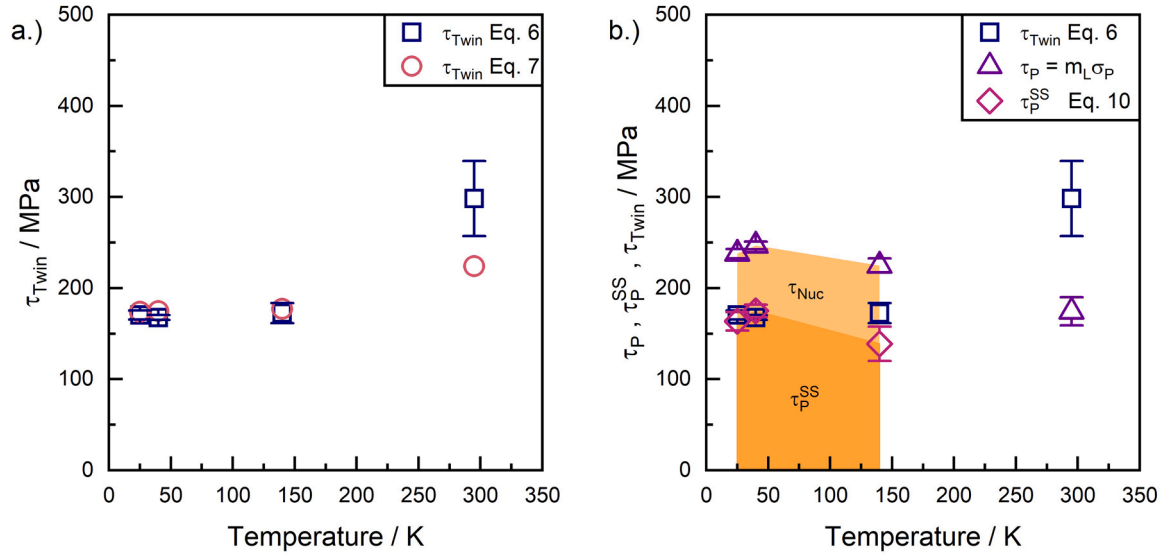

Fig. 7. a.) Critical resolved shear stress for twinning (τ_{Twin}) determined from Eqs. (6),(7) b.) τ_P^{SS} determined according to Eq. (10) in addition to τ_{Twin} determined from Eqs. (6),(7).

$Fe_{40}Mn_{40}Co_{10}Cr_{10}$ [72]. The presented results indicate that the predominant deformation mechanism in metastable *fcc* materials may not be described solely on the basis of the intrinsic SFE.

Recently, Lu et al. [73] pointed out that for slightly negative γ_{isf}^{DFT} values, *fcc* materials may deform by transformation-mediated twinning (TMT). In TMT, first wide SFs and fine $\varepsilon-$ martensite platelets form during deformation. On continued deformation, SFs start to form on the basal plane of $\varepsilon-$ martensite, causing a reversion to *fcc* austenite, that is twin related with the initial austenite. Such formation of SFs in $\varepsilon-$ martensite on deformation has been corroborated for a metastable FeMnC steel by Pramanik et al. [74]. Moreover, Wei et al. [75] confirmed for a FeMnCo MEA via in-situ SEM/EBSD experiments that $\varepsilon-$ martensite reverts to austenite via the formation of basal stacking faults. Since the γ_{isf}^{DFT} values of the FeCoCrNi HEA investigated in the present work fall within the $\gamma_{isf}^{DFT}-$ range where TMT can occur (cf. Fig. 4a in Ref. [73]), it is likely that the apparent stability of *fcc* during deformation is related to the occurrence of TMT.

6. Conclusions

The present study investigated the relation between deformation temperature, experimental as well as theoretical SFE values, and the occurrence of deformation twinning in an *fcc* FeCoCrNi HEA by neutron diffraction, transmission electron microscopy and DFT modeling. The conclusions are:

- Experimentally determined SFE values are positive and decrease with the deformation temperature. On the other hand, SFE values determined from DFT are negative and exhibit a linear dependence on temperature.
- The critical resolved shear stress for Shockley partial dislocations can be inferred from considering the dependence of stacking fault probability on true stress. This critical stress increases with decreasing deformation temperature.
- Contributions of nucleation and propagation to the critical resolved shear stress for Shockley partial dislocations can be identified based on the ratio of experimental and theoretical SFE values. At sub-zero temperatures, propagation, rather than nucleation, of SFs becomes rate determining for continued deformation.
- Correcting experimental SFE values for the contribution of nucleation to the critical resolved shear stress for Shockley partial dislocations yields negative SFE values, which coincide with values predicted by DFT for sub-zero temperatures.

CRediT authorship contribution statement

Konstantin V. Werner: Writing – review & editing, Writing – original draft, Visualization, Methodology, Investigation, Formal analysis, Conceptualization. **Muhammad Naeem:** Writing – review & editing, Writing – original draft, Validation, Investigation, Formal analysis, Conceptualization. **Frank Niessen:** Writing – review & editing, Validation, Investigation. **Li Zhu:** Validation, Formal analysis. **Matteo Villa:** Writing – review & editing, Supervision, Conceptualization. **Xun-Li Wang:** Writing – review & editing, Supervision, Funding acquisition. **Marcel A.J. Somers:** Writing – review & editing, Validation, Supervision, Resources, Funding acquisition, Conceptualization.

Declaration of competing interest

The authors declare that they have no known competing financial interests or personal relationships that could have appeared to influence the work reported in this paper. Co-author Xun-Li Wang is an Editorial Board Member for *Acta Materialia* and was not involved in the editorial review or the decision to publish this article.

Acknowledgements

This work was supported by the Independent Research Fund Denmark (DFF) as part of the project SFETailor (Grant No. 9041-00145B) and in part by the Research Grants Council of the Hong Kong Special Administrative Region (Project No. C1020-21 G). M.N. acknowledges Asia-Oceania Neutron Scattering Association (AONSA) for the AONSA Young Research Fellowship (AONSA-YRF-2022). X.L.W. thanks the Croucher Foundation for the Croucher Senior Research Fellowship (CityU 9509008). The neutron diffraction experiments at the Materials and Life Science Experimental Facility at J-PARC were conducted under user program (proposal numbers 2016B0254, 2017B0142 and 2019A0180).

References

[1] Z. Wu, H. Bei, G.M. Pharr, E.P. George, Temperature dependence of the mechanical properties of equiatomic solid solution alloys with face-centered cubic crystal structures, Acta Mater. 81 (2014) 428–441, https://doi.org/10.1016/j.actamat.2014.08.026.
[2] A. Gali, E.P. George, Tensile properties of high- and medium-entropy alloys, Intermetallics. (Barking) 39 (2013) 74–78, https://doi.org/10.1016/j.intermet.2013.03.018.
[3] F. Otto, A. Dlouhý, C. Somsen, H. Bei, G. Eggeler, E.P. George, The influences of temperature and microstructure on the tensile properties of a CoCrFeMnNi high-entropy alloy, Acta Mater. 61 (2013) 5743–5755, https://doi.org/10.1016/j.actamat.2013.06.018.
[4] G. Laplanche, A. Kostka, C. Reinhart, J. Hunfeld, G. Eggeler, E.P. George, Reasons for the superior mechanical properties of medium-entropy CrCoNi compared to high-entropy CrMnFeCoNi, Acta Mater. 128 (2017) 292–303, https://doi.org/10.1016/j.actamat.2017.02.036.
[5] M. Naeem, H. He, F. Zhang, H. Huang, S. Harjo, T. Kawasaki, B. Wang, S. Lan, Z. Wu, F. Wang, Y. Wu, Z. Lu, Z. Zhang, C.T. Liu, X.L. Wang, Cooperative deformation in high-entropy alloys at ultralow temperatures, Sci. Adv. 6 (2020) 4002–4029, https://doi.org/10.1126/sciadv.aax4002.
[6] B. Yin, S. Yoshida, N. Tsuji, W.A. Curtin, Yield strength and misfit volumes of NiCoCr and implications for short-range-order, Nat. Commun. (2020) 11, https://doi.org/10.1038/s41467-020-16083-1.
[7] S. Yoshida, T. Bhattacharjee, Y. Bai, N. Tsuji, Friction stress and Hall-Petch relationship in CoCrNi equi-atomic medium entropy alloy processed by severe plastic deformation and subsequent annealing, Scr. Mater. 134 (2017) 33–36, https://doi.org/10.1016/j.scriptamat.2017.02.042.
[8] C. Wagner, G. Laplanche, Effects of stacking fault energy and temperature on grain boundary strengthening, intrinsic lattice strength and deformation mechanisms in CrMnFeCoNi high-entropy alloys with different Cr/Ni ratios, Acta Mater. 244 (2023) 118541, https://doi.org/10.1016/j.actamat.2022.118541.
[9] S. Kheiri, H. Mirzadeh, M. Naghizadeh, Tailoring the microstructure and mechanical properties of AISI 316L austenitic stainless steel via cold rolling and reversion annealing, Mater. Sci. Eng. A. 759 (2019) 90–96, https://doi.org/10.1016/J.MSEA.2019.05.028.
[10] M. Naghizadeh, H. Mirzadeh, Effects of grain size on mechanical properties and work-hardening behavior of aisi 304 austenitic stainless steel, Steel Res. Int. 90 (2019) 1900153, https://doi.org/10.1002/srin.201900153.
[11] G. Laplanche, A. Kostka, O.M. Horst, G. Eggeler, E.P. George, Microstructure evolution and critical stress for twinning in the CrMnFeCoNi high-entropy alloy, Acta Mater. 118 (2016) 152–163, https://doi.org/10.1016/j.actamat.2016.07.038.
[12] X. Wu, D. Mayweg, D. Ponge, Z. Li, Microstructure and deformation behavior of two TWIP/TRIP high entropy alloys upon grain refinement, Mater. Sci. Eng. A. 802 (2021) 140661, https://doi.org/10.1016/j.msea.2020.140661.
[13] S. Allain, J.P. Chateau, O. Bouaziz, A physical model of the twinning-induced plasticity effect in a high manganese austenitic steel, Mater. Sci. Eng. A. 387–389 (2004) 143–147, https://doi.org/10.1016/j.msea.2004.01.060.
[14] O. Bouaziz, N. Guelton, Modelling of TWIP effect on work-hardening, Mater. Sci. Eng. A. 319–321 (2001) 246–249, https://doi.org/10.1016/S0921-5093(00)02019-0.
[15] S. Allain, J.P. Chateau, O. Bouaziz, S. Migot, N. Guelton, Correlations between the calculated stacking fault energy and the plasticity mechanisms in Fe-Mn-C alloys, Mater. Sci. Eng. A. 387–389 (2004) 158–162, https://doi.org/10.1016/j.msea.2004.01.059.
[16] Y. Tian, O.I. Gorbatov, A. Borgenstam, A.V. Ruban, P. Hedström, Deformation microstructure and deformation-induced martensite in austenitic Fe-Cr-Ni alloys depending on stacking fault energy, Metall. Mater. Trans. A Phys. Metall. Mater. Sci. 48 (2017) 1–7, https://doi.org/10.1007/s11661-016-3839-2.
[17] G.B. Olson, M. Cohen, A general mechanism of martensitic nucleation: part I. General concepts and the FCC→HCP transformation, Metall. Trans. A. 7 (1976) 1897–1904, https://doi.org/10.1007/BF02654987.
[18] S. Curtze, V.T. Kuokkala, Dependence of tensile deformation behavior of TWIP steels on stacking fault energy, temperature and strain rate, Acta Mater. 58 (2010) 5129–5141, https://doi.org/10.1016/j.actamat.2010.05.049.
[19] T. Yonezawa, K. Suzuki, S. Ooki, A. Hashimoto, The effect of chemical composition and heat treatment conditions on stacking fault energy for Fe-Cr-Ni austenitic

stainless steel, Metall. Mater. Trans. A Phys. Metall. Mater. Sci. 44 (2013) 5884–5896, https://doi.org/10.1007/s11661-013-1943-0.
[20] R.E. Schramm, R.P. Reed, Stacking fault energies of seven commercial austenitic stainless steels, Metall. Trans. A. 6 (1975) 1345–1351, https://doi.org/10.1007/BF02641927.
[21] L. Vitos, J.O. Nilsson, B. Johansson, Alloying effects on the stacking fault energy in austenitic stainless steels from first-principles theory, Acta Mater. 54 (2006) 3821–3826, https://doi.org/10.1016/j.actamat.2006.04.013.
[22] J.X. Yan, Z.J. Zhang, H. Yu, K.Q. Li, Q.M. Hu, J.B. Yang, Z.F. Zhang, Effects of pressure on the generalized stacking fault energy and twinning propensity of face-centered cubic metals, J. Alloys Compd. 866 (2021) 158869, https://doi.org/10.1016/j.jallcom.2021.158869.
[23] S. Kibey, J.B. Liu, D.D. Johnson, H. Sehitoglu, Predicting twinning stress in fcc metals: linking twin-energy pathways to twin nucleation, Acta Mater. 55 (2007) 6843–6851, https://doi.org/10.1016/j.actamat.2007.08.042.
[24] D. Molnár, G. Engberg, W. Li, S. Lu, P. Hedström, S.K. Kwon, L. Vitos, Experimental study of the γ-surface of austenitic stainless steels, Acta Mater. 173 (2019) 34–43, https://doi.org/10.1016/j.actamat.2019.04.057.
[25] S. Wei, C.C. Tasan, Deformation faulting in a metastable CoCrNiW complex concentrated alloy: a case of negative intrinsic stacking fault energy? Acta Mater. 200 (2020) 992–1007, https://doi.org/10.1016/j.actamat.2020.09.056.
[26] X. Sun, S. Lu, R. Xie, X. An, W. Li, T. Zhang, C. Liang, X. Ding, Y. Wang, H. Zhang, L. Vitos, Can experiment determine the stacking fault energy of metastable alloys? Mater. Des. 199 (2021) 109396 https://doi.org/10.1016/j.matdes.2020.109396.
[27] K.V. Werner, F. Niessen, M. Villa, M.A.J. Somers, Experimental validation of negative stacking fault energies in metastable face-centered cubic materials, Appl. Phys. Lett. 119 (2021) 141902, https://doi.org/10.1063/5.0063761.
[28] K.V. Werner, F. Niessen, W. Li, S. Lu, L. Vitos, M. Villa, M.A.J. Somers, Reconciling experimental and theoretical stacking fault energies in face-centered cubic materials with the experimental twinning stress, Materialia (Oxf) 27 (2023) 101708, https://doi.org/10.1016/j.mtla.2023.101708.
[29] M. Shih, J. Miao, M. Mills, M. Ghazisaeidi, Stacking fault energy in concentrated alloys, Nat. Commun. 12 (2021) 1–10, https://doi.org/10.1038/s41467-021-23860-z.
[30] Z. Wang, W. Lu, F. An, M. Song, D. Ponge, D. Raabe, Z. Li, High stress twinning in a compositionally complex steel of very high stacking fault energy, Nat. Commun. 13 (2022) 1–8, https://doi.org/10.1038/s41467-022-31315-2.
[31] Y. Wang, B. Liu, K. Yan, M. Wang, S. Kabra, Y.L. Chiu, D. Dye, P.D. Lee, Y. Liu, B. Cai, Probing deformation mechanisms of a FeCoCrNi high-entropy alloy at 293 and 77 K using *in situ* neutron diffraction, Acta Mater. 154 (2018) 79–89, https://doi.org/10.1016/j.actamat.2018.05.013.
[32] X. Jin, T. Nakamoto, S. Harjo, T. Hemmi, T. Umeno, T. Ogitsu, A. Yamamoto, M. Sugano, K. Aizawa, J. Abe, W. Gong, T. Iwahashi, Development of a cryogenic load frame for the neutron diffractometer at Takumi in Japan Proton Accelerator Research Complex, Rev. Sci. Instrum. 84 (2013) 063106, https://doi.org/10.1063/1.4810010.
[33] R. Oishi-Tomiyasu, M. Yonemura, T. Morishima, Application of matrix decomposition algorithms for singular matrices to the Pawley method in Z-Rietveld, J. Appl. Crystallogr. 45 (2012) 299–308, https://doi.org/10.1107/S0021889812003998.
[34] B. Warren, X-ray Diffraction, Dover Publications, 1990.
[35] R.P. Reed, R.E. Schramm, Relationship between stacking-fault energy and x-ray measurements of stacking-fault probability and microstrain, J. Appl. Phys. 45 (1974) 4705–4711, https://doi.org/10.1063/1.1663122.
[36] P. Soven, Coherent-potential model of substitutional disordered alloys, Phys. Rev. 156 (1967) 809–813, https://doi.org/10.1103/PhysRev.156.809.
[37] L. Vitos, I.A. Abrikosov, B. Johansson, Anisotropic lattice distortions in random alloys from first-principles theory, Phys. Rev. Lett. 87 (2001) 156401–156401–4, https://doi.org/10.1103/PhysRevLett.87.156401.
[38] L. Vitos, The EMTO-CPA Method. Comput. Quantum Mech. Mater. Eng, 1st ed., Springer, London, 2007, pp. 83–94, https://doi.org/10.1007/978-1-84628-951-4_5.
[39] B.L. Gyorffy, A.J. Pindor, J. Staunton, G.M. Stocks, H. Winter, A first-principles theory of ferromagnetic phase transitions in metals, J. Phys. F Met. Phys. 15 (1985) 1337–1386, https://doi.org/10.1088/0305-4608/15/6/018.
[40] W. Li, S. Lu, Q.M. Hu, B. Johansson, S.K. Kwon, M. Grehk, J.Y. Johnsson, L. Vitos, Generalized stacking fault energy of γ-Fe, Philos. Mag. 96 (2016) 524–541, https://doi.org/10.1080/14786435.2016.1140912.
[41] J.P. Perdew, K. Burke, M. Ernzerhof, Generalized gradient approximation made simple, Phys. Rev. Lett. 77 (1996) 3865–3868, https://doi.org/10.1103/PhysRevLett.77.3865.
[42] M. Naeem, H. He, S. Harjo, T. Kawasaki, W. Lin, J.J. Kai, Z. Wu, S. Lan, X.L. Wang, Temperature-dependent hardening contributions in CrFeCoNi high-entropy alloy, Acta Mater. 221 (2021) 117371, https://doi.org/10.1016/j.actamat.2021.117371.
[43] S. Yoshida, T. Ikeuchi, T. Bhattacharjee, Y. Bai, A. Shibata, N. Tsuji, Effect of elemental combination on friction stress and Hall-Petch relationship in face-centered cubic high /medium entropy alloys, Acta Mater. 171 (2019) 201–215, https://doi.org/10.1016/j.actamat.2019.04.017.
[44] M. Schneider, G. Laplanche, Effects of temperature on mechanical properties and deformation mechanisms of the equiatomic CrFeNi medium-entropy alloy, Acta Mater. 204 (2021) 116470, https://doi.org/10.1016/j.actamat.2020.11.012.
[45] I. Gutierrez-Urrutia, S. Zaefferer, D. Raabe, The effect of grain size and grain orientation on deformation twinning in a Fe-22wt.% Mn-0.6wt.% C TWIP steel, Mater. Sci. Eng. A. 527 (2010) 3552–3560, https://doi.org/10.1016/j.msea.2010.02.041.
[46] S.J. Sun, Y.Z. Tian, H.R. Lin, H.J. Yang, X.G. Dong, Y.H. Wang, Z.F. Zhang, Transition of twinning behavior in CoCrFeMnNi high entropy alloy with grain refinement, Mater. Sci. Eng. A. 712 (2018) 603–607, https://doi.org/10.1016/j.msea.2017.12.022.
[47] S.W. Wu, G. Wang, J. Yi, Y.D. Jia, I. Hussain, Q.J. Zhai, P.K. Liaw, Strong grain-size effect on deformation twinning of an Al0.1CoCrFeNi high-entropy alloy, Mater. Res. Lett. 5 (2017) 276–283, https://doi.org/10.1080/21663831.2016.1257514.
[48] Y.F. Shen, N. Jia, Y.D. Wang, X. Sun, L. Zuo, D. Raabe, Suppression of twinning and phase transformation in an ultrafine grained 2 GPa strong metastable austenitic steel: experiment and simulation, Acta Mater. 97 (2015) 305–315, https://doi.org/10.1016/j.actamat.2015.06.053.
[49] J. Chen, F.T. Dong, Z.Y. Liu, G.D. Wang, Grain size dependence of twinning behaviors and resultant cryogenic impact toughness in high manganese austenitic steel, J. Mater. Res. Technol. 10 (2021) 175–187, https://doi.org/10.1016/j.jmrt.2020.12.030.
[50] K.M. Rahman, V.A. Vorontsov, D. Dye, The effect of grain size on the twin initiation stress in a TWIP steel, Acta Mater. 89 (2015) 247–257, https://doi.org/10.1016/j.actamat.2015.02.008.
[51] L. Tang, L. Wang, M. Wang, H. Liu, S. Kabra, Y. Chiu, B. Cai, Synergistic deformation pathways in a TWIP steel at cryogenic temperatures: in situ neutron diffraction, Acta Mater. 200 (2020) 943–958, https://doi.org/10.1016/j.actamat.2020.09.075.
[52] L. Tang, K. Yan, B. Cai, Y. Wang, B. Liu, S. Kabra, M.M. Attallah, Y. Liu, Deformation mechanisms of FeCoCrNiMo0.2 high entropy alloy at 77 and 15 K, Scr. Mater. 178 (2020) 166–170, https://doi.org/10.1016/j.scriptamat.2019.11.026.
[53] I.V. Kireeva, Y.I. Chumlyakov, A.V. Vyrodova, Z.V. Pobedennaya, I. Karaman, Effect of twinning on the orientation dependence of mechanical behaviour and fracture in single crystals of the equiatomic CoCrFeMnNi high-entropy alloy at 77K, Mater. Sci. Eng. A. 784 (2020) 139315, https://doi.org/10.1016/j.msea.2020.139315.
[54] I.V. Kireeva, Y.I. Chumlyakov, Z.V. Pobedennaya, A.V. Vyrodova, I. Karaman, Twinning in [001]-oriented single crystals of CoCrFeMnNi high-entropy alloy at tensile deformation, Mater. Sci. Eng. A. 713 (2018) 253–259, https://doi.org/10.1016/j.msea.2017.12.059.
[55] I.V. Kireeva, Y.I. Chumlyakov, Z.V. Pobedennaya, A.V. Vyrodova, I.V. Kuksgauzen, D.A. Kuksgauzen, Orientation and temperature dependence of a planar slip and twinning in single crystals of Al0.3CoCrFeNi high-entropy alloy, Mater. Sci. Eng. A. 737 (2018) 47–60, https://doi.org/10.1016/j.msea.2018.09.025.
[56] I. Kireeva, Y. Chumlyakov, Z. Pobedennaya, A. Vyrodova, I. Kuksgauzen, D. Kuksgauzen, Twinning and critical resolved shear stresses for twinning in single crystals of high-entropy alloys, AIP Conf. Proc. 2051 (2018) 020123, https://doi.org/10.1063/1.5083366.
[57] W. Abuzaid, H. Sehitoglu, Critical resolved shear stress for slip and twin nucleation in single crystalline FeNiCoCrMn high entropy alloy, Mater. Charact. 129 (2017) 288–299, https://doi.org/10.1016/j.matchar.2017.05.014.
[58] S.F. Liu, Y. Wu, H.T. Wang, J.Y. He, J.B. Liu, C.X. Chen, X.J. Liu, H.T. Wang, Z. P. Lu, Stacking fault energy of face-centered-cubic high entropy alloys, Intermetallics. (Barking) 93 (2018) 269–273, https://doi.org/10.1016/j.intermet.2017.10.004.
[59] A.J. Zaddach, C. Niu, C.C. Koch, D.L. Irving, Mechanical properties and stacking fault energies of NiFeCrCoMn high-entropy alloy, Jom 65 (2013) 1780–1789, https://doi.org/10.1007/s11837-013-0771-4.
[60] S.M.S.S.J. Lee, S.M.S.S.J. Lee, S.M.S.S.J. Lee, J.H. Nam, Y.K. Lee, Tensile properties and deformation mode of Si-added Fe-18Mn-0.6C steels, Acta Mater. 144 (2018) 738–747, https://doi.org/10.1016/j.actamat.2017.11.023.
[61] R.M. Latanision, A.W. Ruff, The temperature dependence of stacking fault energy in Fe-Cr-Ni alloys, Metall. Trans. 2 (1971) 505–509, https://doi.org/10.1007/BF02663341.
[62] S. Huang, W. Li, E. Holmström, S.K. Kwon, O. Eriksson, L. Vitos, Plastic deformation transition in FeCrCoNiAlx high-entropy alloys, Mater. Res. Lett. 7 (2019) 439–445, https://doi.org/10.1080/21663831.2019.1644683.
[63] C. Wagner, A. Ferrari, J. Schreuer, J.P. Couzinié, Y. Ikeda, F. Körmann, G. Eggeler, E.P. George, G. Laplanche, Effects of Cr/Ni ratio on physical properties of Cr-Mn-Fe-Co-Ni high-entropy alloys, Acta Mater. 227 (2022) 117693, https://doi.org/10.1016/j.actamat.2022.117693.
[64] F. Niessen, W. Li, K.V. Werner, S. Lu, L. Vitos, M. Villa, M.A.J. Somers, Ab initio study of the effect of interstitial alloying on the intrinsic stacking fault energy of paramagnetic γ-Fe and austenitic stainless steel, Acta Mater. (2023) 118967, https://doi.org/10.1016/J.ACTAMAT.2023.118967.
[65] E.P. George, W.A. Curtin, C.C. Tasan, High entropy alloys: a focused review of mechanical properties and deformation mechanisms, Acta Mater. 188 (2020) 435–474, https://doi.org/10.1016/j.actamat.2019.12.015.
[66] R.E. Kubilay, W.A. Curtin, Theory of twin strengthening in fcc high entropy alloys, Acta Mater. 216 (2021) 117119, https://doi.org/10.1016/j.actamat.2021.117119.
[67] D.R. Steinmetz, T. Jäpel, B. Wietbrock, P. Eisenlohr, I. Gutierrez-Urrutia, A. Saeed-Akbari, T. Hickel, F. Roters, D. Raabe, A. Saeed–Akbari, T. Hickel, F. Roters, D. Raabe, Revealing the strain-hardening behavior of twinning-induced plasticity steels: theory, simulations, experiments, Acta Mater. 61 (2013) 494–510, https://doi.org/10.1016/j.actamat.2012.09.064.
[68] F. Tranchant, J. Vergnol, J. Grilhé, Twinning in α Cu-A1 crystals: an instability of plastic flow. Strength Met. Alloy. (ICSMA 8), Pergamon, 1989, pp. 167–172, https://doi.org/10.1016/b978-0-08-034804-9.50021-8.
[69] C. Wagner, G. Laplanche, Effect of grain size on critical twinning stress and work hardening behavior in the equiatomic CrMnFeCoNi high-entropy alloy, Int. J. Plast. 166 (2023) 103651, https://doi.org/10.1016/j.ijplas.2023.103651.

[70] B. Neding, O.I. Gorbatov, J.C.C. Tseng, P. Hedström, *In Situ* bulk observations and ab initio calculations revealing the temperature dependence of stacking fault energy in Fe–Cr–Ni alloys, Metall. Mater. Trans. A Phys. Metall. Mater. Sci. 52 (2021) 5357–5366, https://doi.org/10.1007/s11661-021-06473-5.

[71] L. Velterop, R. Delhez, T.H. De Keijser, E.J. Mittemeijer, D. Reefman, X-ray diffraction analysis of stacking and twin faults in f.c.c. metals: a revision and allowance for texture and non-uniform fault probabilities, J. Appl. Crystallogr. 33 (2000) 296–306, https://doi.org/10.1107/S0021889800000133.

[72] S. Picak, J. Liu, C. Hayrettin, W. Nasim, D. Canadinc, K. Xie, Y.I. Chumlyakov, I. V. Kireeva, I. Karaman, Anomalous work hardening behavior of Fe40Mn40Cr10Co10 high entropy alloy single crystals deformed by twinning and slip, Acta Mater. 181 (2019) 555–569, https://doi.org/10.1016/j.actamat.2019.09.048.

[73] S. Lu, X. Sun, Y. Tian, X. An, W. Li, Y. Chen, H. Zhang, L. Vitos, Theory of transformation-mediated twinning, PNAS. Nexus. 2 (2023) 1–11, https://doi.org/10.1093/pnasnexus/pgac282.

[74] S. Pramanik, A.A. Gazder, A.A. Saleh, E.V. Pereloma, Nucleation, coarsening and deformation accommodation mechanisms of ε-martensite in a high manganese steel, Mater. Sci. Eng. A. 731 (2018) 506–519, https://doi.org/10.1016/j.msea.2018.06.024.

[75] S. Wei, M. Xu, J.M. LeBeau, C.C. Tasan, Tuning mechanical metastability in FeMnCo medium entropy alloys and a peek into deformable hexagonal close-packed martensite, Appl. Phys. Lett. 119 (2021) 261905, https://doi.org/10.1063/5.0079981.